Boosting photocurrent of GaInP top-cell for current-matched III-V monolithic multiple-junction solar cells via plasmonic decahedral-shaped Au nanoparticles

Yiming Bai[1, *], Lingling Yan[1], Fuzhi Wang[1], Yun Yang[2,*], Huiyun Liu[3], Zhigang Yin[4], Nuofu Chen[1], Tasawar Hayat[5], Ahmed Alsaedi[5], Zhan'ao Tan[1, *]

[1] *State Key Laboratory of Alternate Electrical Power System with Renewable Energy Sources, North China Electric Power University, Beijing 102206, China*

[2] *Nanomaterials and Chemistry Key Laboratory, Wenzhou University, Wenzhou 325027, China*

[3] *Department of Electronic & Electrical Engineering University College London, London, WC1E 7JE, UK*

[4] *College of Materials Science and Opto-electronic Technology, University of Chinese Academy of Sciences, Beijing 100049, China*

[5] *NAAM Research Group, Faculty of Science, King Abdulaziz University, Jeddah 21589, Saudi Arabia*

[*] Corresponding authors. Tel.: +86 10-61772455; fax: +86 10-61772816.

E-mail: ymbai@ncepu.edu.cn (Y. M. Bai), bachier@163.com (Y. Yang), tanzhanao@ncepu.edu.cn (Z. A. Tan)

Abstract

Unbalanced photocurrent output for each sub-cell in monolithic multiple junction solar cells (MMJ-SCs) reduces the achievable photovoltaic power efficiency (PCE). Here, we first introduce Au decahedra nanoparticles to realize the plasmon-enhanced photo-absorption of GaInP top-cell and achieve the current-matched MMJ-SCs. By simply spin-coating the Au decahedral nanoparticles on the illuminated surface of the devices, the PCEs of the monolithic double junction and triple junction solar cells increase significantly from 27.01% to 28.63% and from 29.88% to 31.90%, respectively. Both the theoretical local electromagnetic distributions and the experimental extinction properties confirm the plasmonic induced absorption enhancement in device performance, and further elucidate the essential reason for photocurrent enhancement derives from the more furious oscillation of free electrons in the vicinity of sharp vertexes for Au decahedra nanoparticles. Our results demonstrate that Au decahedra with sharp vertexes and edges are promising for meliorating the trade-off between light absorption and carrier collection in GaInP top-cell. In addition, this facile and simple strategy also highlights non-annealing treatment and prevents the impurity diffusion at high temperature for MMJ-SCs, and may facilitate other types of solar-harvesting devices.

Key words: Monolithic multiple junction solar cells, Current-matching, Au decahedra nanoparticles, GaInP top-cell

1. Introduction

Monolithic multi-junction solar cells (MMJ-SCs) are solar cells with different bandgap sub-cells in series to realize high efficiency photovoltaic conversion [Xin et al., 2015; Bonnet-Eymard

et al., 2013]. Theoretically, a high up to 50% limiting efficiency can be achieved for GaAs-based MMJ-SCs under the one-sun AM1.5G terrestrial spectrum [Lan and Green, 2016]. However, the 40% efficiency has not been gained for the most common monolithic triple-junction solar cells (MTJ-SCs) utilizing a germanium bottom cell with an (In)GaAs and InGaP middle and top cells respectively [Daneshazarian et al., 2018; Teffah and Zhang, 2017; Espinet-Gonzalez et al., 2015]. This structure of device is very well lattice matched but is not current matched [Fetzer et al., 2004], and two aspects limit the current mismatch. Firstly, the Ge sub-cell with bandgap of 0.67 eV is not a suitable bottom candidate, which absorbs two times more photons than the top two junctions do [Friedman and Olson, 2001]. Secondly, the GaInP top cell with bandgap of 1.9 eV can only absorb the specific spectrum lower than 670 nm [Babaro et al., 2016]. Consequently, the present current-mismatched MTJ-SCs haven't reach the expected efficiency of the current matching models [Mellor et al., 2017].

To realize the current matching in MMJ-SCs, increasing the number of junctions with optimal band gaps seems to be the most promising way [Bremner et al., 2016]. Yet, the breakthrough on four- or more MMJ-SCs is lab-only suffering greatly from the poor quality of each junction and the auxiliary tunnel junctions, with no solution yet for a mass-market offering and launch plans [Datas and Linares, 2017]. Another solution for solving the current mismatching in MMJ-SCs is employing three junctions with more effective bandgaps, but the choice of materials and approaches to do so is very limited due to the lattice-matched requirements and a higher epitaxy technique [Pavelescu et al., 2005]. One of the most desirable approaches for this issue is using GaInNAs compounds with a ~ 1 eV bandgap to replace the Ge bottom cell [Geisz et al., 1998]. Despite massive efforts on fabricating this type of device, the dilute nitride junctions were of poor quality resulting devices with low efficiency [Aho et al., 2014]. In addition, the metamorphic and inverted metamorphic growth are possible to improve current matching but subject to a varying degree of defects and dislocations introduced via the InGaAs buffer layer [Zhang et al., 2016]. Hence, enhancing the photocurrent of GaInP top cell is the simplest and the most effective method for efficient TJ-SCs [Barrigon et al., 2015].

Theoretically, utilizing thicker film to realize full potential light absorption is the easiest approach to realize current matching for MTJ-SCs [Leem et al., 2014]. However, the trade-off between the light absorption and carrier collection remains challenging because the minority diffusion length in GaInP film is greatly limited by the short minority carrier lifetime of a few nanoseconds [Mintairov et al., 2010; Cotal et al., 2009; Park et al., 2014]. Namely, increasing the active layer of GaInP subcell will lead to a low ratio of charge collection, thus resulting in a poorer photovoltaic efficiency. Generally, the widely adopted thickness of GaInP top-cell is in the order of hundreds of nanometers instead of its theoretical thickness of micrometers, leading to insufficient absorption of the incident illumination [Conibeer, 2007]. Furthermore, to gain the cost reduction, the design concept of less material consumption is also promoted recently [Micheli et al., 2016]. Therefore, how to increase photon harvesting of GaInP top cell with the common thickness is still a big challenge.

Plasmonic noble metal nanostructures have been proved effective for meliorating the trade-off and maximizing the light harvesting within the active layer of solar cells, and the cause for this is certainly [Liu et al., 2016]. It's well known that the absorption of photovoltaic devices strongly depends on the incident light path length and is proportional to the local electromagnetic field intensity [Hwang et al., 2017; Atwater and Polman, 2010; Xu et al., 2014]. The introduction of plasmonic nanostructure could induce a strong

scattering of incident light besides the enhanced local electromagnetic field due to the collective oscillation of free electrons. Consequently, lengthening the light path and increasing the incident light absorption ascribe to the interaction between the electrons within the metal nanostructure and the incident light [Wang and He, 2017; Li et al., 2017b; Li et al., 2016; Bai et al., 2014]. Recently, a large number of investigations on various solar cells verify the feasibility of the metal plasmonic nanostructures (MPNs) [Sygletou et al., 2017]. Nevertheless, data are still scarce on exploring the practicability of MPNs for GaAs-based MMJ-SCs because the devices are very sensitive to heat and should never be exposed to temperatures over 500 °C. As we all know that the serious impurity diffusion of the highly doped tunnel junctions at high temperature will cause thermal degradation of GaAs-based MMJ-SCs [Abderrezek et al., 2015; Helmers et al., 2013; Feteha and Eldallal, 2003]. Therefore, MPSs fabricated by physical method with higher annealing temperature seems not to be the favorable method to minimize the dopant diffusion and promote the photocurrent of GaInP top-cell. Nevertheless, this limitation might be overcome by spin-coating of nanoparticles (NPs), which were prepared by chemical method, on GaAs-based MMJ-SCs. It must be emphasized that, advantages of using MPNs prepared by chemical method rather than physical method in MMJ-SCs are as follows: (i) free of the higher annealing temperature; (ii) more kinds of NPs with diversified and complicated geometry since the absorption enhancement depends heavily on the geometry of MPNs [Xu et al., 2016].

To date, Au or Ag NPs with varieties of geometries, covering common sphere, semi-sphere, cube, rod, prism, and complicated octahedron have been used as light trapping structure in solar cells to improve the PCE [Li et al., 2017a; Khodasevych et al. 2015; Bai et al., 2016a]. These studies pointed out that the light trapping capability of the nanostructures has a close relation with the sharp characteristics, such as the vertexes, corners and edges, of the nanostructures in each kind of geometries. The local electromagnetic field near the well-defined vertexes, corners and edges are induced remarkably owning to the aggregation of free electrons distribution when compared with that of the isotropic spherical counterpart, which could be explained by increasing the light scattering efficiency and lowering the self-absorption loss of NPs [Chan et al., 2016]. Given the above, distinct enhancement of PCE for GaAs-based MMJ-SCs is expecting to be achieved upon the introduction of MPNs with sharp corners and edges. Unfortunately, few attempts have been done on this field.

Here, Au decahedral NPs with well-defined vertexes and edges, spherical and ellipsoidal Au NPs were introduced to promote the PCE of GaAs-based MMJ-SCs. It was confirmed experimentally and theoretically that the devices with Au decahedral NPs demonstrate the best property promotions both in the short wavelength enhancement of light absorption and distinct improvement of PCE. The PCE of double-junction and triple-junction devices with Au decahedral NPs reach up to 28.63% and 31.90%. The comparative theoretical simulation of finite difference time domain (FDTD) and the experimental extinction spectra clearly reveal the origin of the short circuit current density promotion. Therefore, it's reasonable to conclude that Au decahedral NPs are more favorable for solving the puzzle between the carrier collection and optical absorption in GaInP top-cell and realization of current-matched monolithic III-V multiple-junction solar cells.

2. Experiments

The lattice-matched monolithic double-junction solar cell (MDJ-SC) and MTJ-SC wafers were

epitaxial grown by metal-organic vapor phase epitaxy (MOVPE), as shown schematically in Fig. 1. The former combines a 1.88 eV $Ga_{0.5}In_{0.5}P$ and a 1.42 eV GaAs sub-cells. The latter contains a 1.90 eV $Ga_{0.51}In_{0.49}P$ top-cell, a 1.40 eV $Ga_{0.99}In_{0.01}As$ middle-cell, and a 0.67 eV Ge bottom-cell. The highly doped and ultra-thin tunnel-junction of p^{++}-GaAs/n^{++}-GaAs in monolithic double-junction solar cells (MDJ-SCs), p^{++}-AlGaAs/n^{++}-GaInP and p^{++}-GaAs/n^{++}-GaAs in MTJ-SCs fully guarantee a low resistance and high current density. The epitaxial growth conditions were guided by references [Friedman et al., 2001; Barrutia et al., 2017, Bai et al., 2016a]. The cross-section SEM images of the MMJ-SCs structure (right in Fig. 1) demonstrate the good morphology and free of crystal defects at interfaces between different layers.

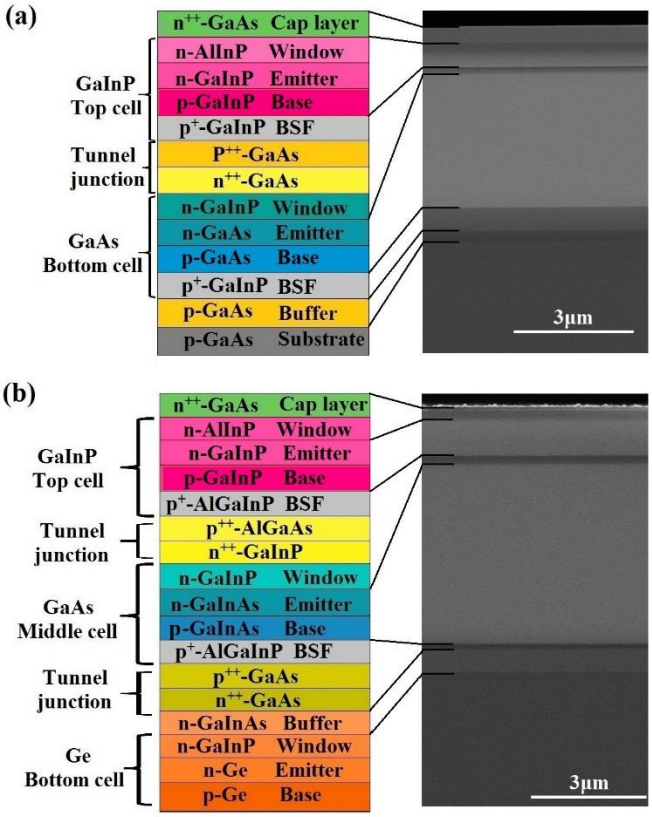

Fig. 1. The schematic layer architectures (left) and their corresponding cross sectional view SEM images (right) for the epitxial structure of GaInP/GaInAs/Ge DJSCs and GaInP/GaInAs/Ge TJSCs, respectively.

The MMJ-SCs chips evaluated in this work were 10×11 mm^2 in size. 1 mm grid pitch of optimal electrode distribution under 1-sun operation was designed for maximum utilization of incident sunlight and decreasing resistance loss. The device processing on photoetching, wet etching, ohmic contacts and anti-reflection coatings were conducted after the theoretical calculation of electrode patterns and the thickness of anti-reflection coatings [Antonio and Steven, 2003; Sze and Ng, 2006]. The Au decahedral NPs were synthesized via the $AgNO_3$-assisted method in accordance with the previous literatures [Fan et al., 2012]. Lastly, the decahedral Au NPs were dip-coated on the surface of MMJ-SCs.

The geometry, size and energy spectrum characterizations of Au NPs were determined by a FeiTecnai G2 F30 transmission electron microscope (TEM) using a carbon-coated copper grid. A

hitachi S4800 field emission scanning electron microscopy (SEM) was used to observe the distribution of Au NPs on the device surface and the cross-section SEM images of MMJ-PSs. The optical properties were investigated using LAMBDA 950 ultraviolet-visible spectrophotometer/near-infrared (UV-Vis/NIR) spectrophotometer.

The current density–voltage (J–V) curves were measured using a Keithley 2400 Source Measure Unit and a New-port 92250A Solar Simulator under one-sun AM1.5 (1000 W/m^2, 25 °C) standard test conditions. As before, the PCE, short-circuit current density (J_{sc}), open circuit voltage (V_{oc}) and fill factor (*FF*) were averaged from 10 individual devices. The performance characterization of external quantum efficiency (EQE) was further tested under the control of QE-R system in air. The intensity of each wavelength was calibrated by the standard single-crystal silicon photovoltaic cell.

3. Results and discussion

3.1. Morphology and optical properties of Au decahedral NPs

It must be emphasized that, the size of NPs as well as geometry is also very vital to enhance the optical absorption of SCs, and the NPs with diameter beyond 50 nm can generate a stronger near-field electromagnetic enhancement due to the surface damping of electrons, radiative scattering and electrodynamic retardation act upon each other [Bai et al., 2014]. To evaluate meticulously the geometry and size features of NPs, Fig. 2a-c present the high-resolution TEM images of the Au decahedral NPs. As can be seen, the exquisite uniformly sized Au decahedral with well-defined vertexes and edges are obtained using the $AgNO_3$-assisted chemical method [Fan et al., 2012]. The mean edge length of Au NPs is about 31.5 nm measured from the representative NPs in Fig. 2c, which is in good accordance with the statistical edge length distribution histogram (the inset in Fig. 2a) analyzed by Image J software. Further, Fig. 2d reveals that the composed element of the decahedral NPs is pure Au, and a very small percentage of carbon and copper elements existed for the usage of carbon coated copper mesh in the TEM measurement. Consequently, it is reasonable to foretell that Au decahedral NPs with sharp tip and suitable size could induce more prominent local filed enhancement and therefore higher photocurrent via spin-coating these NPs on the MMJ-PSs.

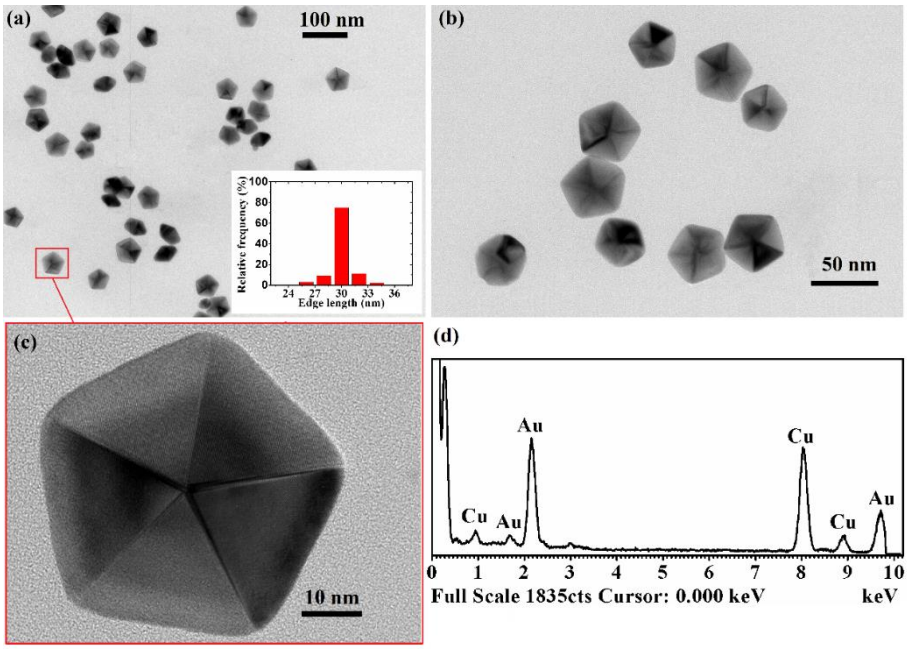

Fig. 2. TEM results of Au decahedral NPs. (a, b) TEM images, (c) high-resolution TEM image showing the representative NPs enclosed by the box in panel (a), (d) energy dispersive X-ray detector spectrum of decahedral NPs.

Fig. 3 shows the distribution of Au decahedra NPs on the surface of MMJ-SCs. In our previous studies [Li et al., 2017a], the Au NPs tend to aggregate when the concentration exceeds 0.8 wt%. Here, the density of Au NPs is 0.75 wt%. The plane-view SEM images confirm that Au decahedra can be well dispersed on the device surface without apparent aggregation, which is in accordance with the results discussed in our pervious investigations [Li et al., 2017a].

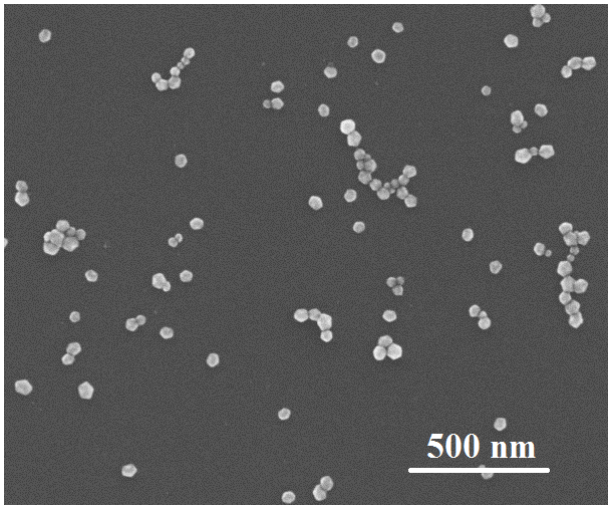

Fig. 3. Plane-view SEM image of the Au decahedral NPs on the surface of MMJ-SCs.

FDTD based on the solutions of Maxwell's equations is an effective approach to get an in-depth understanding about the local electromagnetic field distribution around the Au NPs, and thus assessing their potential function on photocurrent enhancement of SCs. In this work, Au NPs are uniformly distributed on the surface of devices to ensure more efficient light absorption, and a comparison of the near field distribution for Au decahedra, sphere and ellipsoid with the similar size

was shown since we aim to demonstrate the overview of visualized effect for NPs without and with sharp vertices. The wavelength of incident plane wave is 300-900 nm, which corresponds to the wavelength of solar spectrum. The incident field intensity E_0 was set to be 1V/m, and all the grid sizes were 0.5 nm. In addition, the dielectric constants of Au were taken from Palik [Palik, 1998].

Fig. 4 gives the FDTD simulation results of the field intensity distribution of the Au decahedra, sphere and ellipsoid with the similar dimension. Namely, the edge length of the Au decahedra is 31.5 nm, the diameter of the spherical Au NPs is 50 nm, and the principal axes length 2*a*, 2*b* and 2*c* for the ellipsoidal particles are 48, 52 and 25 nm. It appears clearly that the hot spots with pronounced field enhancement can be observed in the vicinity of the sharp vertexes, edges and corners of Au decahedra (Fig. 4a) caused by more furious oscillation of enormous free electrons in comparison with the isotropic spherical NPs (Fig. 4b) and ellipsoidal NPs (Fig. 4c) [Bai et al., 2016b]. Definitely, the stronger near-filed intensity enhancement predicts more incident light absorbing capability and thus boosting the device photocurrent. Furthermore, the local field intensity attenuates obviously as the distance is away from the surface of Au NPs [Yi et al., 2016], which elucidates the mechanism that only the photocurrent enhancement of top-cell can be achieved while that of the middle- and bottom-cells keep invariably. Therefore, two features are beneficial to realize the current-matched MMJ-SCs. The first involves the stronger field enhancement, and the second relates to the near-field intensity decreases exponentially with the distance increasing.

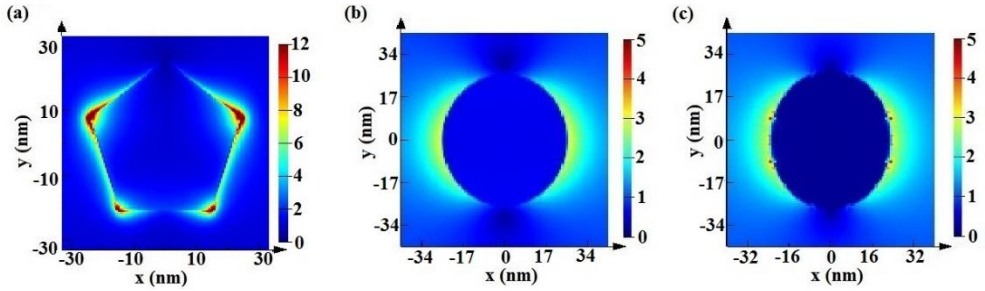

Fig.4. Local field distribution of the Au nanostructures with different morphology, (a) decahedra, (b) sphere, (c) ellipsoid.

To further demonstrate which geometry of NPs is closely match with the absorption wavelength range of GaInP top-cell, Fig. 5a displays the theoretical extinction properties of the three samples calculated from FDTD and the standard AM1.5 solar spectrum for wavelengths of 300-1150 nm. Fig. 5b plots the experimental extinction spectrum of Au NPs in aqueous solution for a direct contrast. As can be seen, the theoretical surface plasmon resonance peaks for Au decahedra, sphere and ellipsoid NPs are 547, 497 and 520 nm, respectively. The experimental counterpart of Au decahedra NPs is 546 nm too, and the increased extinction ability almost disappears for wavelength beyond 600 nm, which indicates that Au decahedra NPs only can boost the optical absorption enhancement of GaInP top-cell with the absorption edge of 670 nm [Babaro et al., 2016]. From the results obtained up till now, both the plasmonic peak and intensity of Au decahedral desire a better light trapping performance as contrast to the sphere and ellipsoid NPs, and thus foretelling a distinct photocurrent enhancement of SCs.

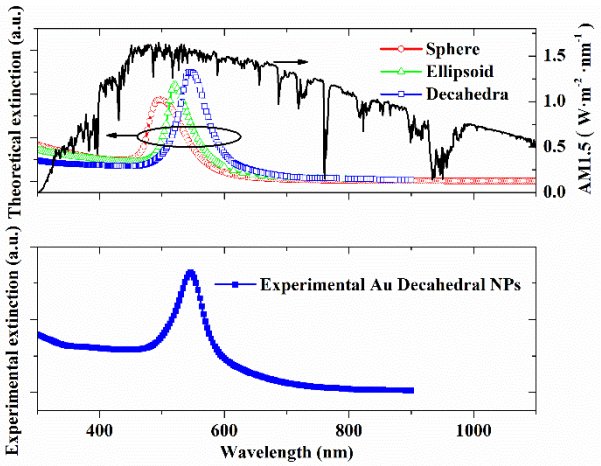

Fig. 5. (a) Theoretical extinction spectra of Au decahedral, spherical and ellipsoidal NPs and the standard AM1.5 solar spectrum for wavelengths of 300-750 nm; (b) experimental extinction spectrum of Au decahedral NPs.

3.2 Current-matched MMJ-SCs induced by Au decahedral NPs

The current-matching effect of the MMJ-SCs induced by Au decahedral NPs is explored by measuring the current density-voltage (J-V) curves of the devices with or without Au decahedral NPs under the illumination of AM 1.5G at 100 mW/cm^2, as presented in Fig. 6. It must be emphasized that the device performance parameters obtained in this work are averaged based upon 10 devices, and the device performance parameters are summarized in Table 1. As the results shown in Fig. 6a, the J_{sc}, the V_{oc}, the *FF* and photovoltaic conversion efficiency (η) for the control device MDJ-SCs without Au decahedral NPs are 12.88 mA/cm^2, 2.48 V, 84.56% and 27.01%, respectively. An obvious performance enhancement of MDJ-SCs can be observed upon the introduction of Au decahedral NPs. The J_{sc} increases to 13.49 mA/cm^2, the *FF* improves to 85.57% while the V_{oc} remains almost the same, leading to a η of 28.63%, which is 6.00% higher than that of the control device.

The corresponding external quantum efficiencies (EQE) and reflection of MDJ-SCs are demonstrated in Fig. 6b. As can be seen, the EQE response characteristic of GaInP top-cell improves distinctly after introducing of Au decahedral NPs, and boosted EQE located from 400 to 600 nm, which is in good agreement with the extinction spectra, but there is negligible effect on other sub-cells [Bai et al., 2016a]. The integrated current for GaInP top-cell without and with Au NPs is 12.70 and 13.31 mA/cm^2, respectively. This is in accordance with the *J-V* results discussed above. This observation verify the reliability of the photovoltaic properties and strongly certify the effect of Au decahedral NPs on enhancing the photocurrent of MTJ-SCs.

The same trend for the performance improvement can be found for the MTJ-SCs with Au decahedral NPs as contrast to the devices without NPs, as presented in Fig. 6c. The control device of MTJ-SCs without Au decahedral NPs afford a PCE of 29.88%, with a J_{sc} of 13.59 mA/cm^2, a V_{oc} of 2.58 V and a *FF* of 85.22%. For the MTJ-SCs with Au decahedral NPs, the V_{oc} is slightly increased to 2.59 V, and the J_{sc} and FF are significantly boosted to 14.36 mA/cm^2 and 85.77%, leading to a PCE of 31.90%, which is increased by 6.76% in comparison with that of the control

device. This more prominent efficiency enhancement further supports our claim that Au decahedral NPs is beneficial to enhance the photocurrent for MMJ-SCs. Furthermore, the standard deviations for the performance data in Table 1 indicate that the processing technology of GaAs-base solar cells are very mature, and the high reproducibility for the performance data makes the evaluation on cell performance reliable. As the EQE results demonstrated in Fig. 6d, the integrated current for GaInP top-cell without and with Au decahedral NPs are 13.48 and 14.29 mA/cm^2, and the EQE intensity enhancements cover a broadband wavelength from 400 to 600 nm. In summary, our results establish that the introduction of Au decahedral NPs is favorable for improving the photocurrent of GaInP top cell, and thus realizing the current-matched MDJ-SCs. Nevertheless, further studies are still necessary to improve the device performance via optimizing the parameters of Au decahedral NPs, which is an area warranting our continuous efforts.

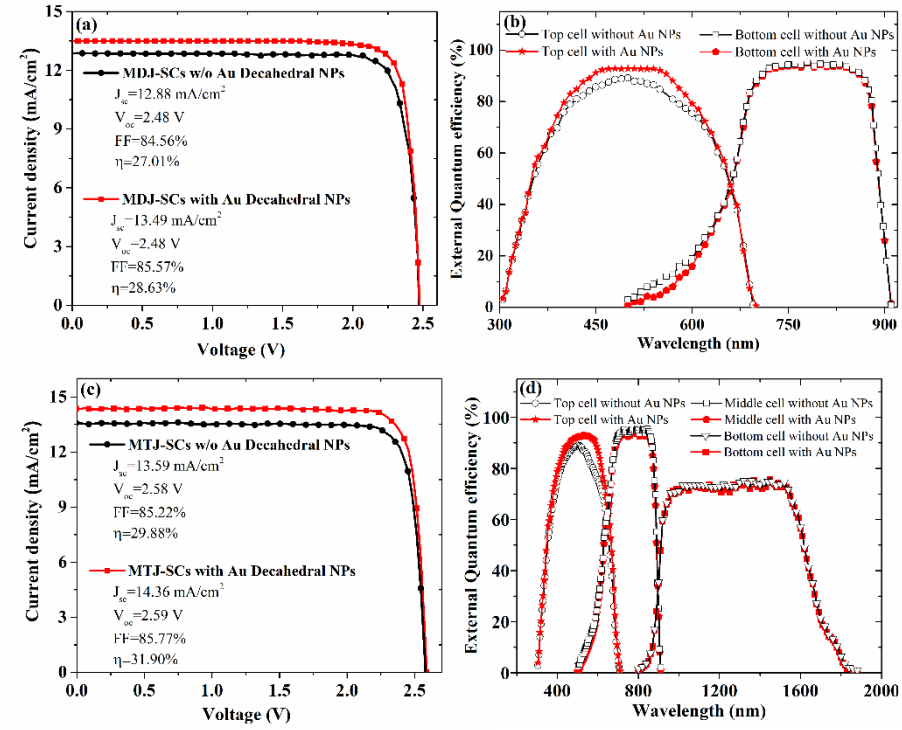

Fig. 6. J-V curves and EQE spectra of (a, b) MDJ-SCs and (c, d) MTJ-SCs. The J-V curves are measured under the illumination of AM 1.5G at 100 mW/cm^2.

Table 1. Device parameters (averaged from 10 individual devices) of MMJ-SCs without and with Au decahedral NPs under the illumination of AM1.5G, 100 mW/cm^2.

Device	w/o or with Au decahedra NPs	J_{sc}(mA/cm^2)	V_{oc}(V)	FF (%)	PCE (%)
MDJ-SCs	w/o	12.88	2.48	84.56	27.01±0.04
	with	13.49	2.48	85.57	28.63±0.06
MTJ-SCs	w/o	13.59	2.58	85.22	29.88±0.05
	with	14.36	2.59	85.77	31.90±0.07

4. Conclusions

In conclusion, Au decahedra NPs fabricated by chemical method have been first introduced to boost the photocurrent of GaInP top cell and therefore current-matched GaInP/GaInAs/Ge MMJ-SCs. The stronger local electromagnetic field enhancement and distinguished optical properties are testified experimentally and theoretically for Au decahedra in comparison to the sphere and ellipsoid, which reveal the essential reasons for the increased photocurrent output. Namely, the more furious oscillation of free electrons in the vicinity of sharp vertexes for Au decahedra could fortify the light absorption of devices. Furthermore, both the near-field intensity-decreasing feature and the extinction features indicate that Au decahedra NPs only can boost the optical absorption enhancement of GaInP top-cell. Under the illumination of AM1.5G 100 mW cm^{-2}, the PCE of MDJ-SCs and MTJ-SCs are increased from 27.01% to 28.63% and from 29.88% to 31.90%, respectively. Our results prove that NPs with sharp vertexes and edges are promising for meliorating the trade-off between light absorption and carrier collection in GaInP top-cell and realizing the current-matched MMJ-SCs.

Acknowledgements

We are grateful to the Natural Science Foundation of China (Grant Nos. 61006050 and 51573042), the Natural Science Foundation of Beijing (Grant No. 2151004), and the Fundamental Research Funds for the Central Universities (Grant Nos. 2016MS50, JB2015RCJ02, 2016YQ06) in China for generous support of our research. Financial support by the China Scholarship Council (Grant No. 201606735041) is gratefully acknowledged.

References

Aho, A., Polojärvi, V., Korpijärvi, V., M., Salmi, J., Tukiainen, A., Laukkanen, P., Guina, M., 2014. Composition dependent growth dynamics in molecular beam epitaxy of GaInNAs solar cells. Sol. Energy Mater. Sol. Cells 124, 150-158.

Antonio, L., Steven, H., 2003. Handbook of photovoltaic science and engineering, in: Swanson, R. M., Photovoltaic Concentrators. John Wiley & Sons Ltd, West Sussex, England, pp. 373-374.

Atwater, H., A., Polman, A., 2010. Plasmonics for improved photovoltaic devices. Nat. Mater. 9, 205-213.

Bai, Y., M., Gao, Z., Chen, N., F., Liu, H., Yao, J., X., Ma, S., Shi, X., Q., 2014. Elimination of small-sized Ag nanoparticles via rapid thermal annealing for high efficiency light trapping structure. Appl. Surf. Sci. 315, 1-7.

Bai, Y., M., Yan, L., L., Wang, J., Su, L., Yin, Z., G., Chen, N., F., Liu, Y., Y., 2016a. Enhancing the photocurrent of top-cell by ellipsoidal silver nanoparticles: towards current-matched GaInP/GaInAs/Ge rtiple-junction solar cells. Nanomaterials 6, 98.

Bai, Y., M., Yan, L., L., Yin, Z., G., Wang, J., Chen, N., F., Chen, J., K., Tan, Z., A., 2016b. Regular hexagonal gold nanoprisms fabricated by a physical method: toward use as ultrasensitive surface-enhanced Raman scattering substrates. Part. Part. Syst. Char. 33, 254-260.

Babaro, J., P., West, K., G., Hamadani, B., H., 2016. Spectral response measurements of

multijunction solar cells with low shunt resistance and breakdown voltages. Energy Sci. Eng. 4, 372.

Barrigon, E., Espinet-Gonzalez, P., Contreras, Y., Rey-Stolle, I., 2015. Implications of low breakdown voltage of component subcells on external quantum efficiency measurements of multijunction solar cells. Prog. Photovolt. Res. Appl. 23, 1597-1607.

Barrutia, L., Barrigon, E., Garcia, I., Rey-Stolle, I., Algora, C., 2017. Effect of Ge autodoping during III-V MOVPE growth on Ge substrates. J. Cryst. Growth 475, 378-383.

Bonnet-Eymard, M., Boccard, M., Bugnon, G., Sculati-Meillaud, F., Despeisse, M., Ballif, C., 2013. Optimized short-circuit current mismatch in multi-junction solar cells. Sol. Energy Mater. Sol. Cells 117, 120-125.

Bremner, S., P., Yi, C., Almansouri, I., Ho-Baillie, A., Green, M., A., 2016. Optimum band gap combinations to make best use of new photovoltaic materials. Sol. Energy 135, 750-757.

Chan, K., Wright, M., Elumalai, N., Uddin, A., Pillai, S., 2016. Plasmonics in organic and perovskite solar cells: optical and electrical effects. Adv. Opt. Mater. 5, 1600698.

Conibeer, G., 2007. Third generation photovoltaics. Mater. Today 10, 42-50.

Cotal, H., Fetzer, C., Boisvert, J., Kinsey, G., King, R., Hebert, P., Yoon, H., Karam, N., 2009. III–V multijunction solar cells for concentrating photovoltaics. Energ. Environ. Sci. 2, 174-192.

Daneshazarian, R., Cuce, E., Cuce, P., M., Sher, F., 2018. Concentrating photovoltaic thermal (CPVT) collectors and systems: theory, performance assessment and applications. Renew. Sustain. Energy. Rev. 81, 473-492.

Datas, A., Linares, P., G., 2017. Monolithic interconnected modules (MIM) for high irradiance photovoltaic energy conversion: a comprehensive review. Renew. Sust. Energ. Rev. 73, 477-495.

Espinet-Gonzalez, P., Rey‐Stolle, I., Ochoa, M., Algora, C., Garcia, I., Barrigon, E., 2015. Analysis of perimeter recombination in the subcells of GaInP/GaAs/Ge triple-junction solar cells. Prog. Photovolt. Res. Appl. 23, 874-882.

Fan, N., N., Yang, Y., Wang, W., F., Zhang, L., J., Chen, W., Zou, C., Huang, S., M., 2012. Selective Etching induces selective growth and controlled formation of various platinum nanostructures by modifying seed surface free energy. Acs Nano 6, 4072.

Fetzer, C., M., King, R., R., Colter, P., C., Edmondsona, K., M., Law, D., C., Stavrides, A., P., Yoon, H., Ermer, J., H., Romero, M., J., Karam, N., H., 2004. High-efficiency metamorphic GaInP/GaInAs/Ge solar cells grown by MOVPE. J. Cryst. Growth 261, 341-348.

Feteha, M., Y., Eldallal, G., M., 2003. The effects of temperature and light concentration on the GaInP/GaAs multijunction solar cell's performance. Renew Energ. 28, 1097-1104.

Friedman, D., J., Olson, J., M., 2001. Analysis of Ge junctions for GaInP/GaAs/Ge three-junction solar cells. Prog. Photovolt. Res. Appl. 9, 179-189.

Geisz, J., F., Friedman, D., J., Olson, J., M., Kurtz, S., R., Keyes, B., M., 1998. Photocurrent of 1 eV GaInNAs lattice-matched to GaAs. J. Cryst. Growth 195, 401-408.

Guter, W., Schone, J., Philipps, S., P., Steiner, M., Siefer, G., Wekkeli, A., Welser, E., Oliva, E., Bett, A., W., Dimroth, F., 2009. Current-matched triple-junction solar cell reaching 41.1% conversion efficiency under concentrated sunlight. Appl. Phys. Lett. 94, 183516.

Helmers, H., Schachtner, M., Bett, A., W., 2013. Influence of temperature and irradiance on triple-junction solar subcells. Sol. Energy Mater. Sol. Cells 116, 144-152.

Hwang, I., Choi, D., Lee, S., Seo, J., H., Kim, K., H., Yoon, I., See, K., 2017. Enhancement of light

absorption in photovoltaic devices using textured PDMS stickers. ACS Appl. Mater. Interfaces 9, 21276-21282.

Khodasevych, I., E., Wang, L., P., Mitchell, A., Rosengarten, G., 2015. Micro‐and nanostructured surfaces for selective solar absorption. Adv. Opt. Mater. 3, 852-881.

Lan, D., C., Green, M., A., 2016. Limiting efficiencies of GaInP/GaAs/Ge up-conversion systems: Addressing the issue of radiative coupling. Appl. Phys. Lett. 109, 42.

Leem, J., W., Yu, J., S., Kim, J., N., Noh, S., K., 2014. Theoretical modeling and optimization of III–V GaInP/GaAs/Ge monolithic triple-junction solar cells. J. Korean Phys. Soc. 64, 1561-1565.

Li, Q., X., Wang, F., Z., Bai, Y., M., Li, X., Yang, Y., Yan, L., L., Hu, S., Q., Zhang, B., Dai, S., Y., Tan, Z., A., 2017a. Decahedral-shaped Au nanoparticles as plasmonic centers for high performance polymer solar cells. Org. Electron. 43, 33-40.

Li, W., C., Ying, Y., Qiao, X., J., Li, Q., Qiao, L., Zheng, J., W., Jiang, L., Q., Che, S., L., 2016. Plasmonic metasurface for light absorption enhancement in GaAs thin film. Plasmonics 11, 1401-1406.

Li, Y., Li, Z., W., Chi, C., Shan, H., Y., Zheng, L., H., Fang, Z., Y., 2017b. Plasmonics of 2D nanomaterials: properties and applications. Adv. Sci. 4, 1600430.

Liu, X., Q., Iocozzia, J., Wang, Y., Cui, X., Chen, Y., W., Zhao, S., Q., Li, Z., Li, Z., Q., 2016. Noble metal-metal oxide nanohybrids with tailored nanostructures for efficient solar energy conversion, photocatalysis and environmental remediation. Energ. Environ. Sci. 10, 402-434.

Mahfoud, M., Fathi, M., Mekhilef, S., Djahli, F., 2015. Effect of temperature on the GaInP/GaAs tandem solar cell performances. Int. J. Energ. Res. 5, 629-634.

Mellor, A., Hylton, N., P., Maier, S., A., Ekins-Daukes, N., 2017. Interstitial light-trapping design for multi-junction solar cells. Sol. Energy Mater. Sol. Cells, 159, 212-218.

Micheli, L., Fernandez, E., F., Almonacid, F., Mallick, T., K., Smestadd, G., P., 2016. Performance, limits and economic perspectives for passive cooling of high concentrator photovoltaics. Sol. Energy Mater. Sol. Cells 153, 164-178.

Mintairov, S., A., Andreev, V., M., Emelyanov, V., M, Kalyuzhnyy, N., A., Timoshina, N., K., Shvarts, M., Z., Lantratov, V., M., 2010. Study of minority carrier diffusion lengths in photoactive layers of multijunction solar cells. Semiconductors 44, 1084-1089.

Palik, E., D., 1998. Handbook of optical constants of solids, Academic Press, London.

Park, K., W., Park, C., Y., Ravindran, S., Kang, S., J., Hwang, H., Y., Jho, Y., D., Jo, Y., R., Kim, B., J., Lee, Y., T., 2014. Enhancement of minority carrier lifetime of GaInP with lateral composition modulation structure grown by molecular beam epitaxy. J. Appl. Phys. 116, 043516-043516-8

Pavelescu, E., M., Wagner, J., Komsa, H., P., Rantala, T., T., Dumitrescu, M., Pessa, M., 2005. Nitrogen incorporation into GaInNAs lattice-matched to GaAs: the effects of growth temperature and thermal annealing. J. Appl. Phys. 98, 083524-083524-4.

Ren, Z., K., Liu, H., H., Liu, Z., Tan, C., S., Aberle, A., G., Buonassisi, T., Peters, I., M., 2017. The GaAs/GaAs/Si solar cell-owards current matching in an integrated two terminal tandem. Sol. Energy Mater. Sol. Cells 160, 94-100.

Sygletou, M., Petridis, C., Kymakis, E., Stratakis, E., 2017. Advanced photonic processes for photovoltaic and energy storage systems. Adv. Mater.1700335.

Sze, S., M., Ng, K., K., 2006. Physics of modern semiconductor devices, 3rd edition, pp. 474-519.

Teffah, K., Zhang, Y., T., 2017. Modeling and experimental research of hybrid PV-thermoelectric system for high concentrated solar energy conversion. Sol. Energy 157, 10-19

Tiwari, B., Hossain, M., J., Bhattacharya, I., 2016. GaP/InGaAs/InGaSb triple junction current matched photovoltaic cell with optimized thickness and quantum efficiency. Sol. Energy 135, 618-624.

Wang, H., P., He, J., H., 2017. Toward highly efficient nanostructured solar cells using concurrent electrical and optical design. Adv. Energy Mater. 1602385.

Xin, G., C., Wang, Y., P., Sun, Y., Huang, Q., W., Zhu, L., 2015. Experimental study of liquid-immersion III–V multi-junction solar cells with dimethyl silicon oil under high concentrations. Energ. Convers. Manage. 94, 169-177.

Xu, X., B., Cui, J., Han, J., B., Zhang, Y., B., Luan, L., Alemuet, G., Wang, Z., Shen, Y., Xiong, D., H., Wei, Z., H., Yang, S., H., Hu, B., Cheng, Y., B., Wang, M., K., 2014. Near field enhanced photocurrent generation in p-type dye-sensitized solar cells. Sci. Rep. 4, 3961.

Xu, Z., H., Liu, Y., L., Ren, F., Q., Yang, F., Ma, D., L., 2016. Development of functional nanostructures and their applications in catalysis and solar cells. Coordin. Chem. Rev. s 320, 153-180.

Yi, Z., Ye, X., Luo, J., S., Kang, X., L., Yi, Y., G., Yi, Y., Huang, J., Jiang, X., D., Tang, Y., J., 2016. Ordered hexagonal nanoplasmonic Au nanoparticle arrays: AAO-assisted thermal treatment synthesis and application as surface-enhanced Raman scattering substrates. Plasmonics 1-8.

Zhang, Y., Q., Wu, Y., Y., Zhao, H., J., Sun, C., Y., Xiao, J., D., Geng, H., B., Xue, J., W., Lu, J., F., Wang, Y., 2016. Degradation behavior of electrical properties of inverted metamorphic tri-junction solar cells under 1 MeV electron irradiation. Sol. Energy Mater. Sol. Cells 157, 861-866.